ROYAL SOCIETY
OF CHEMISTRY

PAPER

Check for updates

Hybrids based on borate-functionalized cellulose nanofibers and noble-metal nanoparticles as sustainable catalysts for environmental applications†

Vicente Esquivel-Peña, [ID] [a] Valentina Guccini, [bc] Sugam Kumar, [b] German Salazar-Alvarez, [ID] [bc] Eduardo Rodríguez de San Miguel [ID] [a] and Josefina de Gyves [ID] *[a]

Polymeric supports from renewable resources such as cellulose nanomaterials are having a direct impact on the development of heterogenous sustainable catalysts. Recently, to increase the potentiality of these materials, research has been oriented towards novel functionalization possibilities. In this study, to increase the stability of cellulose nanofiber films as catalytic supports, by limiting the solubility in water, we report the synthesis of new hybrid catalysts (HC) based on silver, gold, and platinum nanoparticles, and the corresponding bimetallic nanoparticles, supported on cellulose nanofibers (CNFs) cross-linked with borate ions. The catalysts were prepared from metal precursors reduced by the CNFs in an aqueous suspension. Metal nanoparticles supported on CNFs with a spherical shape and a mean size of 9 nm were confirmed by TEM, XRD, and SAXS. Functionalized films of HC-CNFs were obtained by adding a borate solution as a cross-linking agent. Solid-state ^{11}B NMR of films with different cross-linking degrees evidenced the presence of four different boron species of which the bis-chelate is responsible for the cross-linking of the CNFs. Also, it may be concluded that the bis-chelate and the mono-chelates modify the microstructure of the film increasing the water uptake and enhancing the catalytic activity in the reduction of 4-nitrophenol.

1. Introduction

Noble metals form excellent and versatile catalysts used in several important reactions applied in industrial processes. However, since their natural abundance is limited, they are extremely expensive, increasing the need to develop more efficient and innovative catalysts.[1] Using a very thin layer of a noble metal over a non-noble metal nucleus not only reduces the

amount of noble metal used, but has also been proved to modify the catalytic properties, which in many cases are enhanced as a result of the synergistic effects in the crystalline and electronic structures of the materials.[2–4] In the case of Fe/Pt nanoparticles (NPs), when iron is used as the crystal nucleus, the obtained catalysts display multiple advantages such as lower cost and easy recoverability due to the magnetic properties of Fe. Zhang *et al.* have obtained catalysts with a nucleus of amorphous iron coated with a thin layer of Pt (core/shell NPs), supported on carbon. They further reported that the amorphous iron nucleus contains a higher amount of defects in the network, which allows the modulation of the electronic structure to increase the catalytic activity.[5,6]

Heterogeneous catalysis is an important approach to environmental remediation because it reduces the cost and energy requirements of chemical processes. However, the recovery and recyclability of the catalysts from the reaction medium avoiding contamination of the products and preserving the activity are key issues.[7,8] The critical role of the support in the catalytic mechanism has been of great importance in the development of heterogeneous catalysts due to the synergistic effects between the metal and its support.[7] Cellulose, the most abundant natural biopolymer, has recently been proposed as a promising support because of its enormous potential. Efforts have been

[a]*Departamento de Química Analítica, Facultad de Química, UNAM, Ciudad Universitaria, 04510, Ciudad de México, Mexico. E-mail: degyves@unam.mx*

[b]*Department of Materials and Environmental Chemistry Arrhenius Laboratory, Stockholm University, SE-106 91 Stockholm, Sweden*

[c]*Wallenberg Wood Science Center, KTH Royal Institute of Technology, SE-100 44 Stockholm, Sweden*

† Electronic supplementary information (ESI) available: Experimental details for acid digestion of MNPs/CNF samples prior to ICP-OES analysis; details of the SAXS fitting procedure and mathematical expressions (SAXS data analysis); proposed silver reduction mechanisms by TEMPO-CNFs (Scheme S1); AFM characterization of cellulose nanofibers (Fig. S1); metal content of in MNPs/CNF catalysts measured by ICP-OES (Table S1); surface plasmon resonance for metallic and bimetallic NPs (Fig. S2); TEM images of PtNPs as a function of reducing agent (Fig. S3); HRTEM images, electron diffraction pattern and size distribution of Ag, Ag@Au and Ag@Pt NPs/CNF (Fig. S4); SAXS fitting mean size distribution parameters (Table S2); FTIR characterization of CNF-borate cross-linked films (Fig. S5). See DOI: 10.1039/d0ra01528h

directed toward the use of much smaller constituents such as nanofibers (NFs) and nanocrystals for cutting-edge applications because of their remarkable properties including high specific surface area, low density, excellent mechanical properties, thermal stability, low cost, biocompatibility, and biodegradability.[8–24] Cellulose nanofibers (CNFs) are long flexible nanofibers with widths of 5–50 nm and lengths in the micron-to-submicron scale (50–3000 nm).[18] Selective oxidation of the hydroxyl groups to carboxylate groups on the surface of each crystalline cellulose fibril, mediated by 2,2,6,6-tetramethylpiperidine-1-oxyl (TEMPO) and subsequent mechanical treatment allows the formation of CNFs with increased capacity to immobilize catalytic metal species.[16,25–27] Consequently, the combination of metal nanoparticles (MNPs) and nanocellulose as the support gives rise to a new multifunctional material based on a renewable component[14,28–31] that facilitates the removal and recovery of the catalyst from the reaction media.

A general approach to obtain MNPs supported on nanocellulose is based on the solution-phase synthesis of metal nanoparticles *via* the chemical reduction of a metal salt by a reducing agent in the presence of a stabilizer. For example, Chen *et al.* obtained AuNPs immobilized on poly(amidoamine) (PAMAM) dendrimer-cellulose nanocrystals, using sodium borohydride and PAMAM dendrimers as reducing agents, that had good catalytic activity in the reduction of 4-nitrophenol (4-nip) to 4-aminophenol (4-amp).[32] Koga *et al.* synthesized AuNPs, AgNPs, and CuNPs over the crystal surfaces of TEMPO-oxidized tunicate-derived cellulose nanofibrils by using the carboxylate groups as selective sites and sodium borohydride as the reducing agent of the respective metal precursors.[15,16] In addition, other authors have reported the formation of MNPs by taking advantage of the reducing capabilities of nanocellulose or functionalized cellulose.[17,31,33]

Selective TEMPO functionalization of cellulose nanofibers to form C6-carboxylate groups *via* C6-aldehyde groups[25,26] also helps to stabilize their suspensions in water because of the electrostatic repulsion between the carboxylate groups in the fibers[34,35] making them partially soluble in water. While this modification is very useful for the stabilization of a suspension, it is detrimental for applications where CNFs are used in the form of an easily recoverable film. To overcome this issue, Kim *et al.*[36] proposed the cross-linking of CNFs with maleic acid to produce aerogels with water absorbency, noticing an improvement in the network stability in a wet state along with a decrease in the water uptake. Another common cross-linking agent is 1,2,3,4-butanetetracarboxylic acid (BTCA), which tends to create a more glassy and fragile structure with cellulose.[37,38] Both maleic acid and BTCA require the use of sodium hypophosphite as a catalyst and high temperatures. However, even though the ability of borate ions to form esters and anhydrides with polyols and saccharides is well-known, their use as a cross-linking agent for cellulose nanomaterials has not been widely studied. Borate ions reversibly react with alcohols to form borate esters and water. Wicklein *et al.*[22] have reported that the complexation of borate with diols in CNFs is strongly influenced

by the pH, showing an increase in the degree of cross-linking (DC) with an increase in the pH.

In this work, with the aim of obtaining sustainable catalysts, mono- and bimetallic nanoparticles were supported on CNFs cross-linked with borate ions and used in the reduction of 4-nip as a model reaction. Metal (Ag, Au, and Pt) nanoparticles were reduced *in situ* in an aqueous CNF suspension, and it was also possible to obtain bimetallic Ag@Au and Ag@Pt NPs (BNPs) by galvanic replacement. The size and form of the MNPs was determined by TEM, SAXS, STEM, and XRD. The DC was determined by solid-state ^{11}B NMR. Cellulose NFs were characterized by AFM. The best performance was obtained for the catalysts in suspension with 95% conversion within 45 s. A comparison of the catalytic results with previous reports[10,16,39–41] indicated that the catalysts in the film form retained acceptable activity when the CNFs were cross-linked with 5 wt(%) borate ions (95% of conversion in 8 min) and were easily recoverable. These materials are good alternatives for green heterogeneous catalytic processes and sustainable applications.

2. Materials and methods

2.1. Materials

Tetraammineplatinum(II) nitrate ($Pt(NH_3)_4(NO_3)_2$, 99.995%), gold(III) chloride ($AuCl_3$, 99.99%), silver nitrate ($AgNO_3$, ≥99%), 3-aminopropyl triethoxysilane (APTES, 99%), 4-nip ($C_6H_5NO_3$, spectrophotometric grade), sodium borohydride ($NaBH_4$, ≥98.0%), sodium tetraborate ($Na_2B_4O_7$, 99%), sodium bicarbonate ($NaHCO_3$, 99.0%), sodium hypochlorite (NaClO, reagent grade), potassium iodate (KI, ≥99.0%), and ammonia solution 25% (NH_3, HPLC grade) were purchased from Sigma-Aldrich. Nitric acid 65% (HNO_3), hydrochloric acid 35% (HCl) and sodium hydroxide (NaOH, ACS reagent) were purchased from VWR chemicals from the highest purity available. TEMPO radical (free radical, 98%) was obtained from Alfa Aesar. Deionized water (Milli-Q, resistivity 18.2 MΩ cm) was used in all experiments.

2.2. Cellulose-nanofiber production

Cellulose nanofibers were obtained from never dried wood pulp supplied by Domsjö Fabriker AB (Domsjö, Sweden). The pulp was oxidized following the protocol reported by Saito *et al.*[27] First, the suspension was washed with HCl solution at pH 2. Then, 40 g (dry content) of pulp was suspended in 2 L of deionized water and mixed together with the TEMPO catalyst (4 mmol) and sodium bromide (0.04 mol). The pH of the suspension was adjusted to 10 and kept constant during the reaction by the addition of 0.5 mol L^{-1} sodium hydroxide solution. Sodium hypochlorite (80 mmol) was slowly added to the suspension to obtain medium-charged CNFs.

A microfluidizer (M-110EH, Microfluidics Corp, United States), consisting of two large chambers connected in series (400 and 200 μm) fixed at 925 bar and two small chambers (200 and 100 μm) fixed at 1600 bar, was used for the mechanical homogenization of the oxidized celluloses. The cellulose was first passed 3 consecutive times in the large chambers at a fiber

concentration of about 1 wt(%). It was then passed 6 times in the small chambers. The CNFs obtained were 1.7 ± 0.5 nm in height and 507 ± 84 nm in length (see ESI Fig. S1†).

2.3. Synthesis of MNPs using CNFs as reducing agent

To synthesize MNPs, 13.7 mL of a 0.31 wt(%) CNF suspension in water were mixed with 1.5 mL of a 0.05 mol L^{-1} buffer solution (ammonia, pH 9.2, or carbonates, pH 6.3 and 10.3) in a 50 mL round-bottom flask. Then a known volume of a 5 × 10^{-3} mol L^{-1} solution of the metal salt, AgNO$_3$, AuCl$_3$ or Pt(NH$_3$)$_4$(NO$_3$)$_2$, was added to the mixture. For AgNPs and AuNPs, the mixture was heated at 60 °C for 30 min, the reduction mechanism of metal salts by cellulose is presented in Scheme S1.† For the PtNPs, two procedures were followed: a CNF and Pt(II) suspension was either heated at 100 °C under reflux for 6 to 18 h, or the mixture was stirred at 60 °C, and after 15 min, 1 mL of a 0.05 mol L^{-1} NaBH$_4$ solution was added as a reducing agent, after which the suspension was continuously stirred for a further 2 h. Finally, air bubbles were removed in a vacuum chamber and 8 mL of the suspension was placed on a Petri dish (inner diameter 3.5 cm) and dried in a climatic chamber at 30 °C and 50% relative humidity for 3 days to form a film.

Once AgNPs had been synthesized, a known volume of Au(II) or Pt(II) was added dropwise to the AgNPs/CNF suspension at a 4 : 1 molar ratio of Ag : M under stirring. The reaction was allowed to proceed until the Ag was replaced by the second metal, thus forming BNPs.

2.4. Cellulose cross-linking with borate

To improve the mechanical properties of the CNF films, cross-linking with borates was carried out following a procedure described elsewhere.[22] Briefly, the MNPs and BNPs supported on CNFs were suspended and mixed with a sodium tetraborate solution (pH 10) so the final borate concentrations were 1, 3 and 5 wt(%) on dry basis, magnetically stirred for 30 min at room temperature and then placed in a Petri dish to form the films as described before.

2.5. Characterization

The surface charge of the CNFs was determined to be 538 μmol g^{-1} by a conductimetric acid–base titration of the oxidized pulp following an established protocol.[42] The length and height of the CNFs were determined by atomic force microscopy (AFM) under air using a Dimension 3100 SPM (Veeco, United States) in tapping mode. One drop of a 0.0001 wt(%) CNF solution was deposited over a freshly cleaned mica substrate modified with 3-aminopropyl triethoxysilane and blow dried with air after 15 s.

Solid-state ^{11}B high performance decoupling magic angle spinning nuclear magnetic resonance (HPDEC-MAS NMR) spectra of the cross-linked CNF films were recorded with a Brucker Avance-II 300 NMR spectrometer at 96.29 MHz frequency and a spinning rate of 3 kHz. Chemical shifts were referenced externally to boric acid.

The water uptake of the CNF films was measured at room temperature by immersing the films in water for 30 min,

removing the excess water with filter paper, and weighing the film on a balance with 0.01 mg precision. The water uptake was calculated with eqn (1).

$$W\% = \frac{W_{\text{wet}} - W_{\text{dry}}}{W_{\text{dry}}} \times 100 \tag{1}$$

XRD patterns were recorded on an X-ray powder diffractometer (Panalytical X'Pert) using Cu-Kα1 radiation (0.154060 nm) at 45 kV and 40 mA at diffraction angles in the range of 10–80°. The average MNP crystallite size was calculated from the full width at half maximum (FWHM) of the peaks using the Scherrer equation (2), where τ is the average crystallite size, K is a constant with a value of 0.9, λ is the X-ray wavelength, β is the FWHM in radians, and θ is the diffraction angle.

$$\tau = \frac{K\lambda}{\beta \cos \theta} \tag{2}$$

Scanning transmission electron microscopy (STEM) and TEM were used to determine the size and shape of the MNPs and their distribution along the CNFs. Following the dilution and homogenization of the samples, one drop of the suspension was placed on a 300-mesh carbon-coated Cu grid and allowed to dry overnight. STEM images were recorded with a JEOL JSM-7401F instrument at a 20 kV accelerating voltage. TEM images were acquired using a JEOL JEM-2010 TEM with a field emission gun at an accelerating voltage of 200 kV.

The metal content in MNPs/CNF catalyst was measured by inductively coupled plasma-optical emission spectroscopy (ICP-OES) after acid digestion with an iCAP 6000 series ICP spectrometer according to the conditions established by the manufacturer (details in the ESI†).

UV-vis spectroscopy was used to determine the surface plasmon resonance (SPR) properties of the MNPs and to quantify the yield of the reduction of gold using the extinction coefficient of AuNPs.[43,44] The spectra were recorded using a PerkinElmer Lambda 19 UV-vis spectrophotometer. The AuNPs/CNF suspension was placed in a quartz cuvette of 1 cm path length and the spectra were recorded against a blank of CNF suspension.

The size distribution of the nanoparticles was probed by the small-angle X-ray scattering (SAXS) experiment carried out using GALAXI (Gallium Anode Low-Angle X-ray Instrument), a small angle X-ray diffractometer at Jülich Centre for Neutron Science (JCNS), Germany. GALAXI utilizes a Bruker AXS Metal Jet as the laboratory X-ray source while the scattered X-rays are collected using a Dectris Pilatus 1M detector. A monochromatic X-ray beam (wavelength ∼ 0.13414 nm) was made incident on the samples and the scattering data were measured at two sample-to-detector distances (83 cm and 353 cm) to cover a wide scattering vector (magnitude) range of about 0.04 to 10 nm^{-1}.

2.6. Catalytic activity test

The reduction of 4-nip to 4-amp was used as a model reaction to determine the catalytic activity of the MNPs supported on CNFs. 2 mL of a freshly prepared aqueous solution of 4-nip (5 ×

10^{-5} mol L^{-1}) was mixed with 200 μL of NaBH$_4$ (0.22 mol L^{-1}) in a quartz cuvette, then 10 μL of the MNPs/CNF suspension was added. The samples were stirred, and the concentration of 4-nip was determined as a function of time by UV-vis spectrometry (n = 3). Several blank experiments were performed under the same conditions with a sample containing the same components but without the MNPs. To evaluate the catalytic activity of the films the procedure was performed using 20 mL of the 4-nip solutions mixed with 2 mL of the NaBH$_4$ solution, then 2 to 3 mg of the selected films as the catalyst were immersed in the solution and the samples were stirred in an orbital shaker at 250 rpm (n = 3).

3. Results and discussion

3.1. Synthesis and characterization of MNPs using CNFs as reducing agent

Thermal activation was necessary to synthesize MNPs using CNFs as a reducing agent; after mixing the metal precursor with CNFs no changes were observed until the temperature reached 50 °C. At this point, a change in the color indicated the reduction of the metal precursor (red for gold and yellow for silver). Controlling the pH during the synthesis was also very important. If the pH decreased below 5, due to the release of CO$_2$ from the buffer, it caused the CNFs to start to agglomerate, which facilitated the aggregation of the MNPs as can be seen in the changes in SPR (Fig. S2†). The particle sizes of the AgNPs and AuNPs determined by TEM were 9.0 ± 1.2 nm and 25.1 ± 9.5 nm, respectively (Fig. 1). For a fixed reaction time of 30 min and under the conditions stated in section 2.3 (Synthesis of MNPs using CNFs as reducing agent), a faster reduction was observed for Au than for Ag. The larger particle size and broader

size distribution of the Au may be a consequence of nuclei growth over time.[45]

To obtain PtNPs using CNFs as the reducing agent, the reaction needed to proceed for a longer time, and the use of an NH$_4^+$/NH$_3$ buffer solution (pH 9.3) was required to prevent the formation of platinum(II) hydroxide and promote the formation of amine complexes. After 6 h of reaction at 100 °C, only 30% of the total Pt was reduced; a small improvement in the yield was achieved after a reaction time of 18 h. XRD measurements revealed the formation of the metallic phase with a mean crystal size of 10 ± 2 nm. Sodium borohydride was used as a reducing agent to improve the reduction yield, leading to instant and complete reduction of Pt(II). A dendrite morphology of the PtNPs was observed when the reduction was performed at room temperature, and spheroidal nanoparticles were obtained when the reduction was performed at 60 °C (Fig. S3†).

Galvanic replacement of silver was carried out to minimize the amount of platinum and gold used in the bimetallic catalysts. The reaction proceeded at room temperature, under magnetic stirring with the dropwise addition of the second metal to the AgNPs/CNF suspension. No significant changes were observed in particle size by TEM and a log-normal size distribution for the AgNPs was obtained. This is typical for the reduction of metal ions with green agents[28,46–49] (Fig. S4†). This distribution did not change after galvanic replacement, indicating that AgNPs were the main component of the MNPs.[50,51] The chemical composition of the BNPs was determined to be 3.87 ± 0.47 Ag/Au molar ratio for Ag@Au NPs/CNF, and 5.25 ± 0.17 Ag/Pt molar ratio for Ag@Pt NPs/CNF by ICP-OES (Table S1†).

SAXS was used to obtain statistical size distribution data to estimate the turnover frequency (TOF) values needed for the
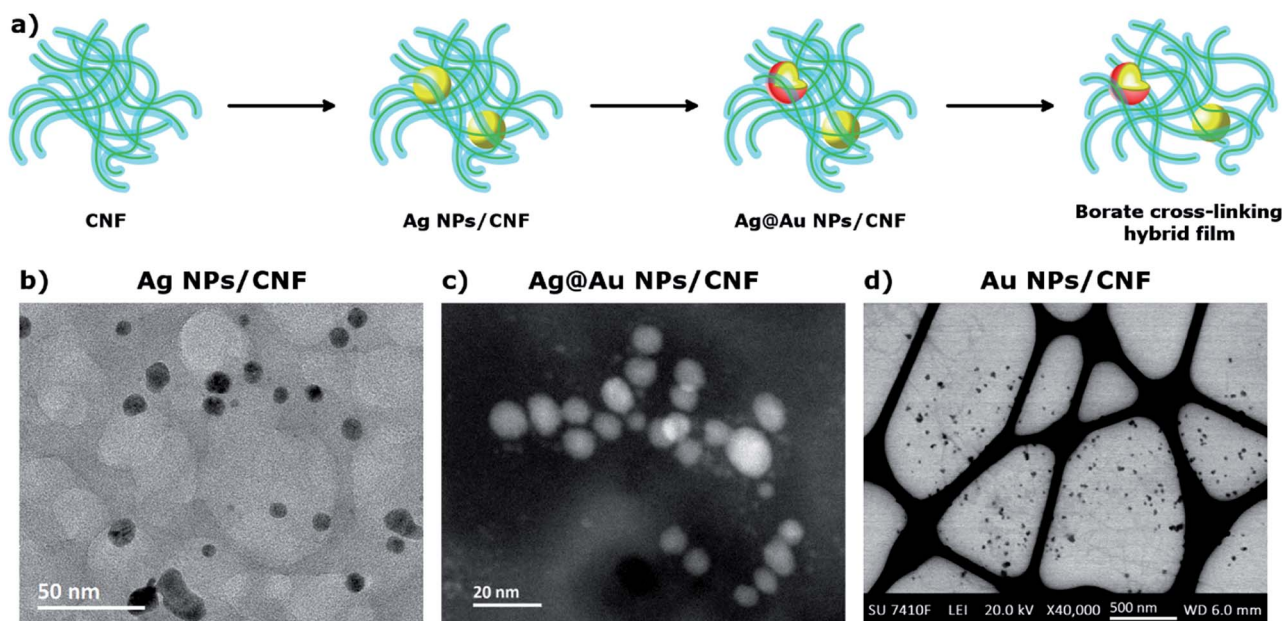

Fig. 1 (a) Representation of the synthesis of metallic and bimetallic nanoparticles with CNFs, (b) TEM image of AgNPs/CNF, (c) STEM high-angle annular dark-field image of Ag@Au NPs/CNF, and (d) STEM-in-SEM image of AuNPs supported on CNFs.
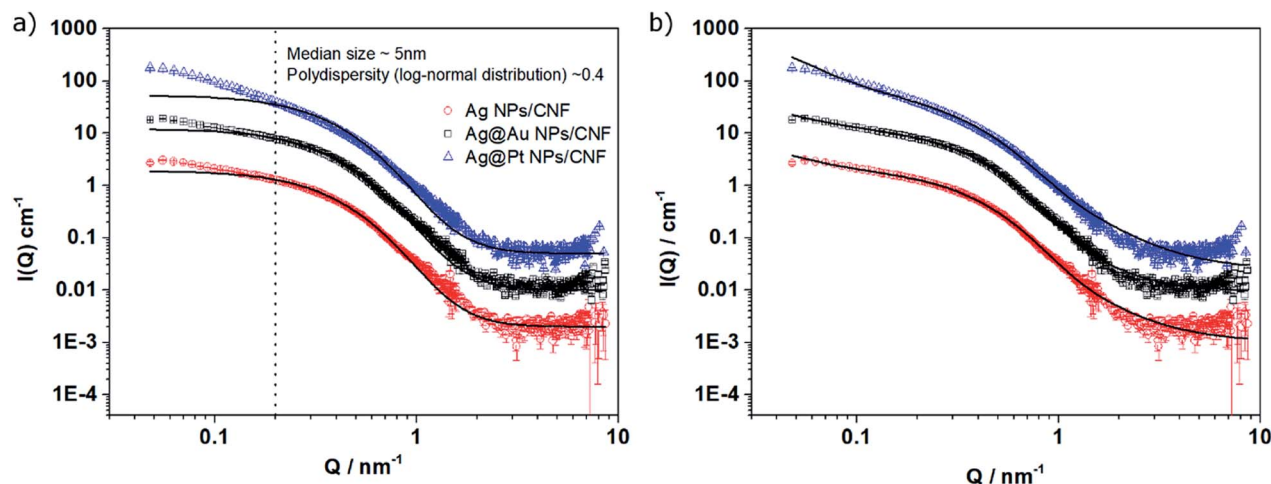
Fig. 2 Small-angle X-ray scattering intensity profiles for the Ag, Ag@Au and Ag@Pt NPs/CNF catalysts analyzed by considering the existence of (a) polydispersed spherical particles only (the fitted curves do not reproduce the experimental data for Q values lower than 0.2 nm^{-1}, dotted line) and, (b) isolated nanoparticles together with small nanoparticles aggregates of mass-fractal morphology. Empty symbols are experimental data and black solid lines are the fitting results. The curves are vertically shifted (Ag@Au × 5 and Ag@Pt × 25) so that each system can be clearly observed.

precise determination of the catalytic activity. The data for the three nanoparticle systems were first analyzed by considering the presence of isolated individual polydisperse spherical nanoparticles (un-aggregated, Fig. 2a). The fitting model reproduced the scattering profiles in the intermediate- and high-Q region ($Q > 0.2$ nm^{-1}) but did not account for the low-Q scattering intensity (Fig. 2a). In contrast, assuming the presence of isolated nanoparticles together with a small fraction of nanoparticle aggregates, as was observed in the TEM images, allowed a good correlation between the experimental data and the fitting model for the three systems analyzed (Fig. 2b). The details of the fitting procedure including mathematical expressions are provided in the ESI† and the fitted mean size

distribution parameters (mean diameter and dispersity) are listed in Table S2.†

3.2. CNF cross-linking with borate ions

To obtain a non-soluble CNF film in water, avoiding the disaggregation of the fibers, the cross-linking with borates was performed, following the methodology described by Wicklein *et al.*,[22] by forming borate esters with the hydroxyl groups of the cellulose nanofibers, as evidenced by FTIR spectroscopy (Fig. S5†). Fig. 3a shows the spectra of solid-state ^{11}B NMR for films with different content of borate as cross-linker. After deconvolution of the signals, we propose the presence of four boron-species: the unreacted borate ion/boric acid ($B(OH)_4^-$/
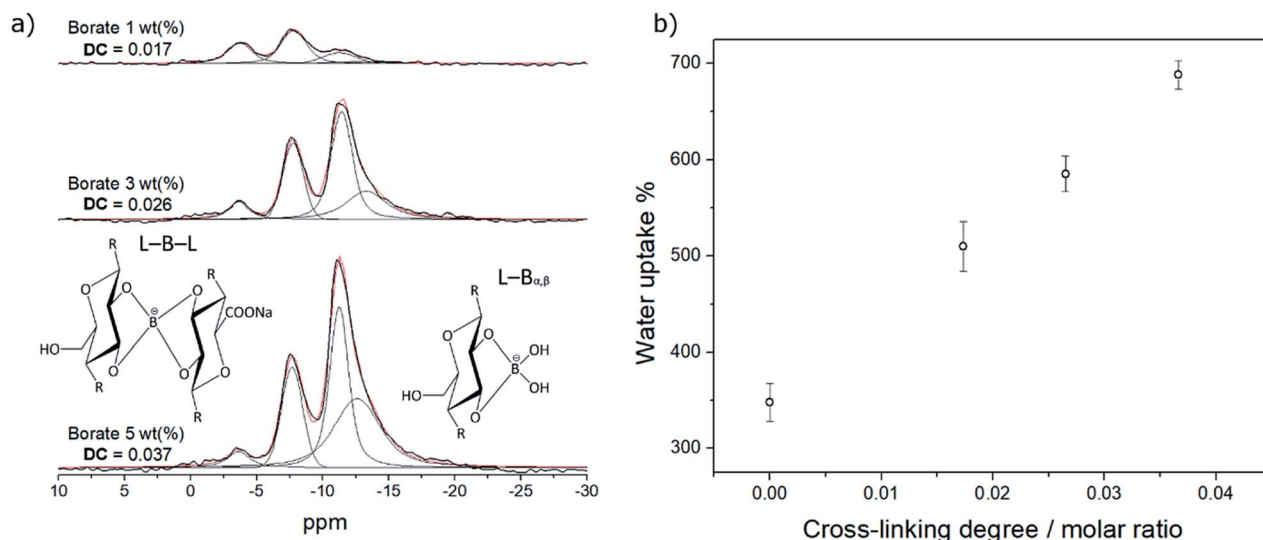

Fig. 3 (a) Solid-state ^{11}B NMR spectra for CNF films cross-linked with different content of borate, and (b) water uptake of the CNF films as a function of the degree of cross-linking.
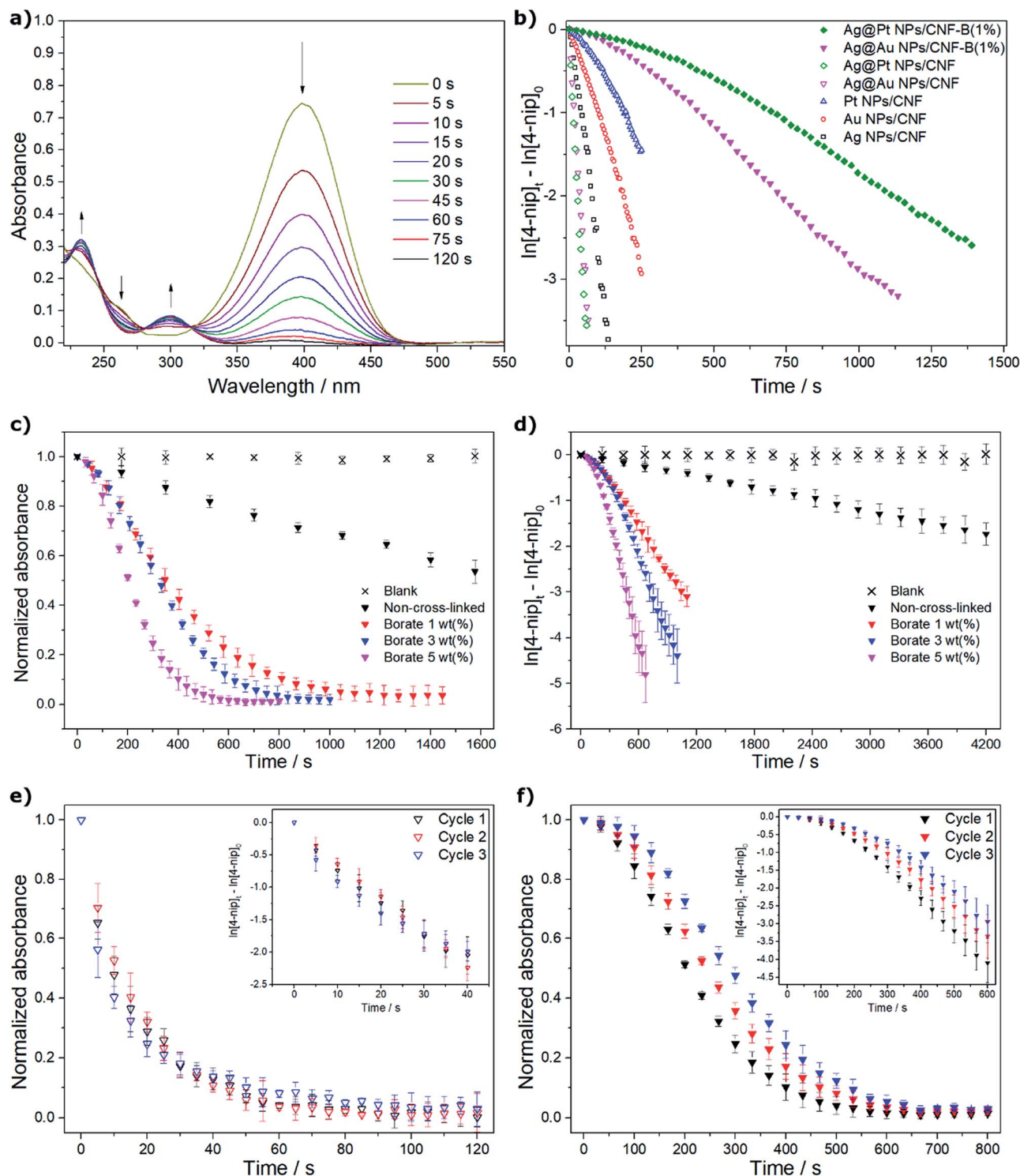
Paper

Fig. 4   Results for the reduction of 4-nip (4.5×10^{-5} mol L^{-1}) with NaBH$_4$ (0.2 mol L^{-1}): (a) UV-vis spectra in the presence of 10 µL of a Ag@Au NPs/CNF 0.26 wt(%) suspension of the catalyst; (b) apparent rate constants for the suspensions of the obtained catalysts (empty symbols) and CNF-borate cross-linked films of bimetallic catalysts (Ag@Au NPs/CNF-B(1%) and Ag@Pt NPs/CNF-B(1%), filled symbols) fitted to a pseudo-first-order kinetic model; (c) profile of the catalytic performance of Ag@Au NPs/CNF-B films as a function of the cross-linker content; (d) pseudo-first-order kinetic model fitting of Ag@Au NPs/CNF-B films as a function of the cross-linker content; (e) consecutive catalytic cycles for the Ag@Au NPs/CNF catalyst suspension, and (f) consecutive catalytic cycles for the Ag@Au NPs/CNF-B(5%) film.

B(OH)$_3$, around −3.7 ppm); a bis-chelate (L–B–L, around −7.6 ppm) and two mono-chelates, alpha-beta mono-chelate (L–B$_{\alpha,\beta}$, around −11.2 ppm) and a small contribution of the alpha-gamma mono-chelate (L–B$_{\alpha,\gamma}$, around −12.6 ppm). Chemical shifts are in good agreement with the literature.[22,52–56] The DC, defined as the molar ratio between the bis-chelate and the

Table 1 Comparison of the catalytic activity of recent reports of MNPs/cellulose nanomaterial catalysts for the reduction of 4-nip

Catalyst	Molar ratio NaBH$_4$/4-nip/M (mol/mol/mol)	TOF (h^{-1})	k_{app} (s^{-1})	Reference
Pt NPs/CNF suspension	14 353/30/1	1038 ± 203	0.0046 ± 0.0010	This work
Au NPs/CNF suspension	8553/18/1	2403 ± 285	0.0111 ± 0.0010	This work
Ag NPs/CNF suspension	2241/45/1	10 205 ± 350	0.0277 ± 0.0012	This work
Ag@Pt NPs/CNF suspension	17 738/36/1	42 202 ± 647	0.0642 ± 0.0038	This work
Ag@Au NPs/CNF suspension	22 087/47/1	45 079 ± 540	0.0536 ± 0.0030	This work
Ag@Pt NPs/CNF-B(1%) film	1774/4/1	352 ± 34	0.0023 ± 0.0009	This work
Ag@Au NPs/CNF-B(1%) film	2209/5/1	461 ± 42	0.0028 ± 0.0006	This work
Ag@Au NPs/CNF-B(3%) film	2209/5/1	576 ± 57	0.0052 ± 0.0007	This work
Ag@Au NPs/CNF-B(5%) film	2209/5/1	811 ± 66	0.0077 ± 0.0003	This work
Au NPs/CNF suspension	150000/150/1	563	0.0059	Koga et al.[16]
Au NPs/CNF suspension	36 000/180/1	657	0.0026	Azetsu et al.[10]
Au NPs/CNC suspension	9720/30/1	109	0.0020	Wu et al.[40]
Au NPs/CNC suspension	9794/3093/1	641	0.0147	Yan et al.[41]
Au NPs/CNC film	12/0.3/1	531	0.0033	Eisa et al.[39]
Ag NPs/CNC film	9/0.23/1	420	0.0040	Eisa et al.[39]

monomer (glucose), increased as the total borate content increased. In addition, the amount of the mono-chelates raised significantly. An increase in the water uptake of the CNF films was observed after cross-linking (Fig. 3b) from ~350% for non-cross-linked CNF films to ~700% for the films with the highest DC (0.037). Moreover, the disaggregation of the fibers in aqueous solution was no longer observed after the cross-linking as determined by UV-vis spectrometry.

The increase in water uptake can be attributed to the hydrophilicity of borate ions and the mono-chelates, which can interact with water molecules by solvation mechanisms.[57] These water molecules can form channels that allow the interaction between reactants and MNPs in the interior of the films, facilitating the mass transfer from the solution to the film and vice versa. It is also important to note that the cross-linked films retain water for a much longer time. These features are very important for heterogeneous catalysis because they allow the interaction between the metal nanoparticles in the interior of the film with the reagents.

3.3. Catalytic activity tests

The catalytic tests were carried out as indicated in the Experimental section. The progress of the reaction was monitored by UV-vis spectroscopy. A decrease in the absorption band of 4-nip was observed as a function of time at 400 nm while an absorption band at 298 nm appeared, indicating the formation of 4-amp (Fig. 4a). The results were fitted to a first-order kinetic model for the conversion of 4-nip (Fig. 4b). It can be seen that the suspended catalysts had a higher activity for the conversion of 4-nip than the borate-cross-linked films. This result can be explained on the basis of a decrease in the number of active sites accessible to the reactants. It is also remarkable that bimetallic systems are more active than the monometallic. This can be attributed to the interaction between the two metals or the galvanic displacement procedure, which tends to create porous structures when the metals have non-equal valences.[58] The best results were obtained with the Ag@Au NPs/CNF

system. Fig. 4c and d show the catalytic activity for the films as a function of the DC. It is important to note that in the film formed without cross-linking, TOF values for the reduction of 4-nip were very low, while the TOF values for the cross-linked films were enhanced at least 10 times. Three independent catalytic cycles were performed to evaluate the stability of the catalyst in suspensions and in films. No statistically significant changes were found for the suspensions and a small decrease in the rate constant (around 20%) was observed for the films (Fig. 4e and f). As can be seen, no evidence of poisoning of the catalyst was observed, consistent with the preservation of the kinetic model for more than 3 half-life times.

A comparison of similar recently reported catalytic systems with those synthesized in this work is presented in Table 1.[10,16,39–41] For the suspensions, the rate constants and TOF values were higher for the studied bimetallic systems, likely because of the good distribution of the catalyst in the CNFs and/or the small nanoparticle size. Even though the catalytic activity was lower in the film form, it was still comparable with those in the suspended form. The great advantage of the film form is the possibility to easily recover the catalyst from the reaction medium and thus prevent the contamination of the product.

4. Conclusions

Metallic (Ag, Au, and Pt) and bimetallic (Ag@Au and Ag@Pt) nanoparticles were successfully obtained on cellulose nanofibers by a facile and controlled procedure. Small nanoparticles with a log-normal size distribution were obtained. Electron microscopy indicated the formation of spherical nanoparticles with a mean diameter of ca. 9.0 nm. These metal and bimetallic nanoparticles were highly active for the reduction of 4-nip to 4-amp at room temperature under mild conditions, retaining the same performance for at least 3 cycles. The materials obtained by cross-linking the MNPs/CNF catalysts with borate ions were used to prepare films that demonstrated an upgraded performance because of the improved stability and water uptake

which can be attributed to the borate mono-chelate species that can interact with water molecules by solvation mechanisms. The procedure allowed the production of catalysts in a controllable and reproducible manner by adjusting the pH and temperature of the aqueous reaction media without the use of organic solvents supported on an abundant, renewable material with high specific surface area. The catalysts can be easily recovered after use without contamination of the products or reaction media, and, consequently, are potentially applicable in other green heterogeneous catalytic processes.

Conflicts of interest

There are no conflicts to declare.

Acknowledgements

References

1 L. Mora-Tamez, V. Esquivel-Peña, A. L. Ocampo, E. Rodriguez de San Miguel, D. Grande and J. de Gyves, *ChemSusChem*, 2017, **10**, 1482–1493.

2 V. Esquivel-Peña, J. Bastos-Arrieta, M. Muñoz, L. Mora-Tamez, N. M. Munguía-Acevedo, A. L. Ocampo and J. de Gyves, *SN Appl. Sci.*, 2019, **1**, 347.

3 X. Teng, D. Black, N. J. Watkins, Y. Gao and H. Yang, *Nano Lett.*, 2003, **3**, 261–264.

4 C. J. Zhong and M. M. Maye, *Adv. Mater.*, 2001, **13**, 1507–1511.

5 T. Toda, H. Igarashi and M. Watanabe, *J. Electroanal. Chem.*, 1999, **460**, 258–262.

6 X.-B. Zhang, J.-M. Yan, S. Han, H. Shioyama and Q. Xu, *J. Am. Chem. Soc.*, 2009, **131**, 2778–2779.

7 D. Astruc, F. Lu and J. R. Aranzaes, *Angew. Chem., Int. Ed.*, 2005, **44**, 7852–7872.

8 A. Fukuoka and P. L. Dhepe, *Chem. Rec.*, 2009, **9**, 224–235.

9 M. Abidi, A. Iram, M. Furkan and A. Naeem, *Int. J. Biol. Macromol.*, 2017, **98**, 459–468.

10 A. Azetsu, H. Koga, A. Isogai and T. Kitaoka, *Catalysts*, 2011, **1**, 83–96.

11 I. Diez, P. Eronen, M. Osterberg, M. B. Linder, O. Ikkala and R. H. A. Ras, *Macromol. Biosci.*, 2011, **11**, 1185–1191.

12 R. M. El-Shishtawy, A. M. Asiri, N. A. M. Abdelwahed and M. M. Al-Otaibi, *Cellulose*, 2011, **18**, 75–82.

13 L. Johnson, W. Thielemans and D. A. Walsh, *Green Chem.*, 2011, **13**, 1686–1693.

14 M. Kaushik and A. Moores, *Green Chem.*, 2016, **18**, 622–637.

15 H. Koga, A. Azetsu, E. Tokunaga, T. Saito, A. Isogai and T. Kitaoka, *J. Mater. Chem.*, 2012, **22**, 5538–5542.

16 H. Koga, E. Tokunaga, M. Hidaka, Y. Umemura, T. Saito, A. Isogai and T. Kitaoka, *Chem. Commun.*, 2010, **46**, 8567–8569.

17 X. B. Lin, M. Wu, S. Kuga, T. Endo and Y. Huang, *Polym. J.*, 2016, **48**, 919–923.

18 R. J. Moon, A. Martini, J. Nairn, J. Simonsen and J. Youngblood, *Chem. Soc. Rev.*, 2011, **40**, 3941–3994.

19 C. Noonan, M. Tajvidi, A. H. Tayeb, M. Shahinpoor and S. E. Tabatabaie, *Materials*, 2019, **12**, 1269.

20 A. H. Tayeb, E. Amini, S. Ghasemi and M. Tajvidi, *Molecules*, 2018, **23**, 2684.

21 U. Vainio, K. Pirkkalainen, K. Kisko, G. Goerigk, N. E. Kotelnikova and R. Serimaa, *Eur. Phys. J. D*, 2007, **42**, 93–101.

22 B. Wicklein, D. Kocjan, F. Carosio, G. Camino and L. Bergstrom, *Chem. Mater.*, 2016, **28**, 1985–1989.

23 B. Wicklein and G. Salazar-Alvarez, *J. Mater. Chem. A*, 2013, **1**, 5469–5478.

24 H. Zhou, P. Lv, X. Lu, X. Hou, M. Zhao, J. Huang, X. Xia and Q. Wei, *ChemSusChem*, 2019, **12**, 5075–5080.

25 A. Isogai, T. Saito and H. Fukuzumi, *Nanoscale*, 2011, **3**, 71–85.

26 T. Saito and A. Isogai, *Colloids Surf., A*, 2006, **289**, 219–225.

27 T. Saito, S. Kimura, Y. Nishiyama and A. Isogai, *Biomacromolecules*, 2007, **8**, 2485–2491.

28 G. Biliuta and S. Coseri, *Coord. Chem. Rev.*, 2019, **383**, 155–173.

29 H. Dong and J. P. Hinestroza, *ACS Appl. Mater. Interfaces*, 2009, **1**, 797–803.

30 J. H. He, T. Kunitake and A. Nakao, *Chem. Mater.*, 2003, **15**, 4401–4406.

31 X. B. Lin, M. Wu, D. Y. Wu, S. Kuga, T. Endo and Y. Huang, *Green Chem.*, 2011, **13**, 283–287.

32 L. Chen, W. J. Cao, P. J. Quinlan, R. M. Berry and K. C. Tam, *ACS Sustainable Chem. Eng.*, 2015, **3**, 978–985.

33 K. Benaissi, L. Johnson, D. A. Walsh and W. Thielemans, *Green Chem.*, 2010, **12**, 220–222.

34 S. Montanari, M. Rountani, L. Heux and M. R. Vignon, *Macromolecules*, 2005, **38**, 1665–1671.

35 T. Saito, Y. Nishiyama, J. L. Putaux, M. Vignon and A. Isogai, *Biomacromolecules*, 2006, **7**, 1687–1691.

36 C. Kim, H. Youn and H. Lee, *Cellulose*, 2015, **22**, 3715–3724.

37 O. Sauperl, K. Stana-Kleinschek and V. Ribitsch, *Text. Res. J.*, 2009, **79**, 780–791.

38 C. C. Wang and C. C. Chen, *J. Appl. Polym. Sci.*, 2005, **97**, 2450–2456.

39 W. H. Eisa, A. M. Abdelgawad and O. J. Rojas, *ACS Sustainable Chem. Eng.*, 2018, **6**, 3974–3983.

40 X. D. Wu, C. H. Lu, Z. H. Zhou, G. P. Yuan, R. Xiong and X. X. Zhang, *Environ. Sci.: Nano*, 2014, **1**, 71–79.

41 W. Yan, C. Chen, L. Wang, D. Zhang, A. J. Li, Z. Yao and L. Y. Shi, *Carbohydr. Polym.*, 2016, **140**, 66–73.

42 Scandinavian Pulp, Paper and Board, *SCAN-CM 65-02*, 2002.

43 A. I. Dolinnyi, *Colloid J.*, 2017, **79**, 611–620.

44 W. Haiss, N. T. K. Thanh, J. Aveyard and D. G. Fernig, *Anal. Chem.*, 2007, **79**, 4215–4221.

45 K. An and G. A. Somorjai, *Chemcatchem*, 2012, **4**, 1512–1524.

46 T. A. J. de Souza, L. R. R. Souza and L. P. Franchi, *Ecotoxicol. Environ. Saf.*, 2019, **171**, 691–700.

47 S. Iravani, *Green Chem.*, 2011, **13**, 2638–2650.

48 H. S. Kim, Y. S. Seo, K. Kim, J. W. Han, Y. Park and S. Cho, *Nanoscale Res. Lett.*, 2016, **11**, 230.

49 M. P. Patil and G. D. Kim, *Appl. Microbiol. Biotechnol.*, 2017, **101**, 79–92.

50 H. Jing and H. Wang, *Chem. Mater.*, 2015, **27**, 2172–2180.

51 X. Zhang, G. Y. Zhang, B. D. Zhang and Z. H. Su, *Langmuir*, 2013, **29**, 6722–6727.

52 M. Bishop, N. Shahid, J. Yang and A. R. Barron, *Dalton Trans.*, 2004, 2621–2634, DOI: 10.1039/B406952H.

53 S. Geng, F. U. Shah, P. Liu, O. N. Antzutkin and K. Oksman, *RSC Adv.*, 2017, **7**, 7483–7491.

54 G. R. Kennedy and M. J. How, *Carbohydr. Res.*, 1973, **28**, 13–19.

55 Y. Miyazaki, K. Yoshimura, Y. Miura, H. Sakashita and K. Ishimaru, *Polyhedron*, 2003, **22**, 909–916.

56 M. Van Duin, J. A. Peters, A. P. G. Kieboom and H. Van Bekkum, *Tetrahedron*, 1985, **41**, 3411–3421.

57 H. DeFrancesco, J. Dudley and A. Coca, in *Boron Reagents in Synthesis*, American Chemical Society, 2016, vol. 1236, ch. 1, pp. 1–25.

58 M. H. Oh, T. Yu, S. H. Yu, B. Lim, K. T. Ko, M. G. Willinger, D. H. Seo, B. H. Kim, M. G. Cho, J. H. Park, K. Kang, Y. E. Sung, N. Pinna and T. Hyeon, *Science*, 2013, **340**, 964–968.